Observation of breather resonances in Josephson ladders

M. Schuster, P. Binder, and A. V. Ustinov
Physikalisches Institut III, Universität Erlangen-Nürnberg, Erwin-Rommel-Straße 1, 91058 Erlangen, Germany
(Received 23 April 2001; published 19 December 2001)

We report experimental observation of resonances excited by nonlinear localized states (rotobreathers) in Josephson junction ladders. The rotobreathers are found to persist in a frequency range that allows for their resonant interaction with linear electromagnetic modes in the ladders. This interaction leads to nearly constant voltage steps on the current-voltage characteristics. We also present numerical simulations that agree well with experimental data and confirm the resonant interaction between breathers and linear waves. Resonances occur at the base frequency as well as higher harmonics of the linear modes. The observed substructures on the resonances are attributed to the cavity modes for the ladders. Both experimental and simulated current-voltage characteristics show good quantitative agreement with an analytically calculated dispersion relation for linear electromagnetic modes.

DOI: 10.1103/PhysRevE.65.016606 PACS number(s): 05.45.Yv, 63.20.Pw, 63.20.Ry, 74.50.+r

I. INTRODUCTION

In recent years, there has been rising interest towards the phenomenon of dynamic localization in homogeneous, yet discrete nonlinear lattices [1,2]. While substantial progress was made on the analytic and numerical edge, it has happened only recently when the first experimental evidences for intrinsic localized modes (also known as discrete breathers) were reported. Discrete breathers were found in coupled optical wave guides [3], low-dimensional crystals [4], antiferromagnetic materials [5], and arrays of coupled small Josephson junctions, so-called Josephson ladders [6,7].

Depending on the type of ''particles'' forming a lattice, discrete breathers may be formed of either *vibrational*, or *rotational* localized modes. The latter, also named *rotobreathers*, are present in lattices constructed of rotors such as pendulums or spins. Rotobreathers correspond to states where the kinetic energy is stored in one or a few whirling sites, while the remaining lattice oscillates with an amplitude that exponentially decays away from the breather center.

A nice example for a nearly ideal rotor is a small Josephson junction. An underdamped, current biased junction is well described within the resistively-capacitively-shunted junction (RCSJ) model [8]. Its dynamic behavior, characterized by the superconducting phase difference φ, is given by the simple equation

$$\ddot{\varphi}+\alpha\dot{\varphi}+\sin\varphi=\gamma, \tag{1}$$

which is identical to the dynamic equation for the angle φ of a damped pendulum subject to a constant torque γ. For a Josephson junction, Eq. (1) is obtained when time is measured in units of the inverse plasma frequency ω_p^{-1}. $\gamma=I/I_c$ is the bias current I normalized to the junction critical current I_c. The damping parameter $\alpha=\sqrt{\Phi_0/2\pi I_c R^2 C}$ is typically small ($\alpha\ll 1$). R is the junction subgap resistance, C is the junction capacitance, and Φ_0 is the magnetic flux quantum. The junction parameters may be specified in a wide range in fabrication and can be tuned during experiment.

For the range $0<\gamma<1$, Eq. (1) has a static solution $\varphi=\arcsin\gamma$. A dynamic solution with $\langle\dot{\varphi}\rangle\approx\gamma/\alpha$ exists down to the ''retrapping'' current $\gamma_r=4\alpha/\pi<1$. Here, $\langle\cdot\rangle$ represents the average in respect to time. The static solution represents a junction in superconducting (''*S*'') state with a constant phase difference, while the dynamic solution characterizes a resistive (''whirling'') junction with φ increasing with time (''*R*'' state). The simultaneous presence of these two different states for a certain range of the external parameter γ is the principal reason for the existence of rotobreathers in arrays of coupled Josephson junctions.

Floría *et al.* [9] proposed a special array, the so-called Josephson ladder, as a relatively simple system in which rotobreathers should be observed.

A schematic view of a Josephson ladder is given in Fig. 1(a). Crosses indicate Josephson junctions, straight lines refer to superconducting electrodes. Arrowheads sketch the direction of external bias currents. The depicted ladder consists of eleven vertical junctions arranged in parallel. These junctions are interconnected via superconducting leads, interrupted by *horizontal* junctions. One cell of the ladder is formed by two horizontal and two vertical junctions. If the horizontal and vertical junctions differ in parameters, the ladder is *anisotropic*. The anisotropy parameter η is defined as

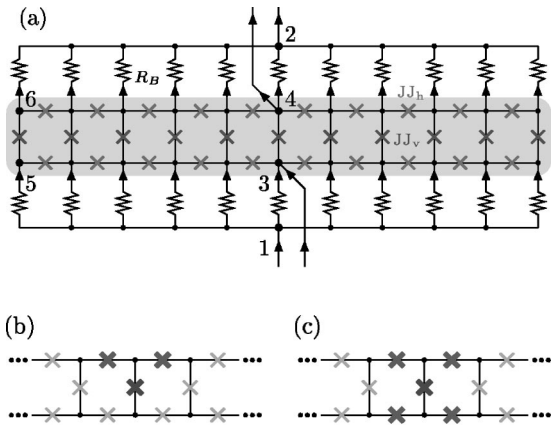

FIG. 1. (a) Schematic of a Josephson ladder (central shaded area) and the biasing circuit (upper and lower nonshaded parts) as described in the text. The type $A1$ (b) and $B1$ (c) breather states are studied in this paper. Bold crosses indicate resistive junctions.

the ratio of the horizontal and vertical junction critical currents, $\eta = I_{c,h}/I_{c,v}$.

The vertical junctions can be biased homogeneously by injecting equal DC-currents I into every node of the lower-electrode row and extracting the same currents at every node of the upper row. In an experiment, this is realized by injecting the current I_B into node 1 of the biasing circuit and extracting the same current from node 2. If the resistors R_B are large in comparison to the resistances of the Josephson junctions, the same normalized currents $\gamma = I/I_c = I_B/[I_c(N+1)]$ are fed into every ladder node, where N is the number of ladder cells.

A rotobreather is formed inside the Josephson ladder if one or a few vertical junctions are in the resistive R state, while the remaining vertical junctions reside in the S state. The R state of the junction is accompanied by a voltage drop across this junction. In order to meet Kirchhoff's voltage conservation law, at least one more junction inside the loop containing the whirling vertical one must also exhibit a nonzero voltage. Depending on the number of whirling junctions inside a loop, different breather types are distinguished in Josephson ladders. Figures 1(b) and 1(c) show two elementary types, the ''asymmetric'' or type A breather, and the ''symmetric'' or type B breather. The *size* of a breather (indicated by the number behind its letter, e.g., $A1$, $A2$, etc.) is given by the number of resistive vertical junctions. However, we want to note that this rough classification does not take into account the exact internal dynamic state of the breather.

A breather may be detected inside a Josephson ladder by measuring the voltage drops between two different vertical junctions of the ladder, e.g., between the center nodes 3 and 4, and between the boundary nodes 5 and 6. If a breather is present in the center of the ladder, a finite voltage will be detected in 3–4, while the voltage across 5–6 is zero.

A large variety of different rotobreather states has been observed and studied in experiments [6,7,10] and in numerical simulations [11–13]. The experiments reported so far concentrated on the principal identification of different states and the study of their stability regions in relation to bias current.

Apart from breathers, Josephson ladders also exhibit dynamical states like electromagnetic cavity modes and traveling magnetic vortices [14,15]. The cavity modes correspond to small amplitude oscillatory eigenmodes of the lattice of Josephson junctions. A dispersion relation for such linear modes was derived and verified in experiment in Ref. [14].

Up to now, experimental breather investigations were focused on cases where the frequencies of the breather states were above the linear mode spectrum. However, it has been found numerically in Ref. [11] that the interaction with extended lattice modes may be survived by a breather and leads to observable resonant steps in current-voltage characteristics. Miroshnichenko *et al.* [12] recently performed numerical studies of resonances between type A breathers and lattice modes, showing that step positions on current-voltage curves may be mapped by the linear wave dispersion relation.

In this paper, we report on the experimental observation of resonances of extended modes with both type A and type B breathers. Furthermore, we present numerical simulations that are in good agreement with the experimental results and dispersion analysis.

II. MODELING JOSEPHSON LADDER DYNAMICS

The dynamical variables for a Josephson ladder are the superconducting phase differences across the upper horizontal junctions $\tilde{\psi}_n$, the vertical junctions φ_n, and the lower-horizontal junctions ψ_n. Within the RCSJ model for a single junction, its dynamics are governed by Eq. (1). Together with Kirchhoff's current conservation law for each node and the fluxoid quantization in each cell of the ladder, a set of equations for the time evolution of the Josephson phases in the ladder may be derived as in [12,14,16]

$$\ddot{\varphi}_n + \alpha\dot{\varphi}_n + \sin\varphi_n = \gamma + \frac{1}{\beta_L}(\Delta\varphi_n + \nabla\psi_{n-1} - \nabla\tilde{\psi}_{n-1}),$$

$$\ddot{\psi}_n + \alpha\dot{\psi}_n + \sin\psi_n = -\frac{1}{\eta\beta_L}(\nabla\varphi_n + \psi_n - \tilde{\psi}_n),$$

$$\ddot{\tilde{\psi}}_n + \alpha\dot{\tilde{\psi}}_n + \sin\tilde{\psi}_n = \frac{1}{\eta\beta_L}(\nabla\varphi_n + \psi_n - \tilde{\psi}_n). \tag{2}$$

Here, the discreteness parameter $\beta_L = 2\pi L I_c/\Phi_0$ is the ratio of the self inductance of a cell L and the Josephson inductance $\Phi_0/2\pi I_c$ of a vertical junction. ∇ and Δ represent the discrete first derivative, $\nabla f_n = f_{n+1} - f_n$, and the discrete Laplacian, $\Delta f_n = f_{n-1} - 2f_n + f_{n+1}$, respectively. n is an integer representing the cell number. For open boundary systems, without externally applied magnetic fields, the proper equations for the boundary phases φ_1 and φ_{N+1} are obtained by putting $\psi_0 = \tilde{\psi}_0 = \psi_{N+1} = \tilde{\psi}_{N+1} = 0$, $\varphi_0 = \varphi_1$, and $\varphi_{N+2} = \varphi_{N+1}$, where N is the number of cells of the ladder.

To determine the spectrum of extended small-amplitude linear modes, Eqs. (2) are linearized around a suitable ground state. When the ladder is homogeneously biased by a current γ, this ground state is characterized by $\varphi_n = \arcsin\gamma$ for all n. Inserting the ansatz

$$\varphi_n = \Phi e^{i(qn-\omega t)}, \tag{3a}$$

$$\psi_n = \Psi e^{i(qn-\omega t)}, \quad \text{and} \tag{3b}$$

$$\tilde{\psi}_n = \tilde{\Psi} e^{i(qn-\omega t)}, \tag{3c}$$

and neglecting damping ($\alpha = 0$), the relation

$$\omega_{\pm}^2 = F \pm \sqrt{F^2 - G} \tag{4}$$

is obtained [12,14], where $F = 1/2 + 1/(\eta\beta_L) + 1/2\sqrt{1-\gamma^2} + 1/\beta_L(1-\cos q)$ and $G = [1 + 2/(\eta\beta_L)]\sqrt{1-\gamma^2} + 2/\beta_L(1-\cos q)$. An additional mode is represented by $\omega_0 = 1$.

Relation (4) describes a lower, almost dispersion-free branch ω_- and an upper branch ω_+ with $\Psi = -\tilde{\Psi}$ [12]. Since any ladder is of finite size, only a limited number of wave vectors is allowed. For an N-cell open-ended ladder, $N+1$ vertical and $2N$ horizontal junctions are present. Con-

sidering linear oscillations of the vertical junctions, the $N+1$ cavity modes correspond to the wave numbers

$$q_l = \frac{l\pi}{N+1} \tag{5}$$

with $0 \leqslant l \leqslant N$.

III. DC MODEL FOR ROTOBREATHERS

In this section, we briefly remind the reader of the previously obtained analytical relations for current-voltage characteristics of rotobreathers in Josephson ladders [6,7,10–12]. Herein, only DC effects are taken into account, while possible interactions with linear modes are neglected.

For a single Josephson junction, the current-voltage characteristics in R state is given by $v \approx \gamma/\alpha$, where $v = \langle \dot{\varphi} \rangle$ is the normalized voltage. This does not change for a Josephson ladder with all vertical junctions in R state and all horizontal junctions in S state. However, for a breather state, the voltage drop $v_v = \langle \dot{\varphi} \rangle$ across a resistive vertical junction at fixed bias current is lower than for a single uncoupled junction. This can be easily understood since a part of the injected bias current is flowing across the breather ''boundaries,'' that are the neighboring horizontal junctions.

Using a network of resistors (the junctions in R state) and superconductors (junctions in S state), the resistance of a breather state may be determined analytically. The vertical voltage drop v_v at the breather site is then related to the homogeneous bias current γ as [6,7]

$$v_v = \frac{\gamma}{\alpha} \frac{k}{k + l\eta}, \tag{6}$$

where k is the number of resistive vertical junctions, $l=2$ for type A breathers, and $l=1$ for type B breathers. In this treatment, the bias resistors are assumed to be large in comparison to the junction normal resistance. If this assumption is dropped, Eq. (6) has to be modified [10,11].

For a type A breather, the horizontal voltage drop $v_h = v_v$ due to Kirchhoff's voltage law. For the type B breather, the only constraint is $v_n + \tilde{v}_h = v_v$. In the simplest case, the absolute values of the upper- and lower-horizontal voltages are identical and equal to half of the vertical voltage. Yet this is not always the rule. For the type A breather, we define the breather frequency $\Omega = v_v$, while for the type B breather, three different junction frequencies $\Omega_v = v_v$ (vertical), $\Omega_h = v_h$ (upper horizontal), and $\tilde{\Omega}_h = \tilde{v}_h$ (lower horizontal) have to be considered. When frequency-dependent dissipation, e.g., due to resonances, sets in, deviations from the simple ohmic current-voltage relation (6) appear.

IV. EXPERIMENTAL RESULTS

We performed experiments with niobium-based Josephson ladders fabricated at Hypres [17]. The layout [see Fig. 1 (a)] is almost identical to the one described in Ref. [10]. The main difference of samples studied in the present paper from that of Ref. [10] is the critical current density, which is substantially lower, about 100 A/cm^2.

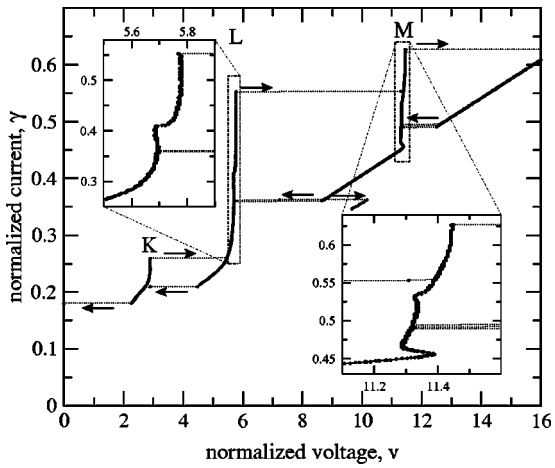

FIG. 2. Experimental current-voltage characteristics of a $B1$ rotobreather in a Josephson ladder. The curve was obtained by multiple current sweeps. The insets show magnifications of the L and M resonance branches. The K branch corresponds to an $A1$ rotobreather.

Measurements were performed in liquid helium at a temperature of $T=4.2$ K. We show data measured from a 10 cell open-ended Josephson ladder of anisotropy $\eta=0.49$. At the measurement temperature, the critical current of a single vertical junction is $I_c = 20.5\,\mu$A, and the self inductance of one cell is $L=10$ pH, which translates to a discreteness parameter of $\beta_L = 0.62$. The junction capacitance is $C=0.95$ pF, and the damping is $\alpha=0.025$. The bias current was injected through resistors with $R_B = 32\,\Omega$.

In the experiments, current-voltage curves of the Josephson ladder were obtained by sweeping the uniformly supplied bias current I_B (injected through the nodes 1 and 2 in Fig. 1) and measuring the voltage drop V_{3-4} between nodes 3 and 4. A breather state may be created in experiment by locally applying a bias current I_L between nodes 3 and 4. Once the breather is produced, I_L is decreased to zero while I_B is turned on. The creation procedure is described in detail in Ref. [7]. We found that such a local biasing usually leads to the formation of a type B breather. For the formation of type A breathers, an alternative biasing technique [18] was used: we apply a bias current $\tilde{I}_L$ between nodes 3 and 2, which breaks the symmetry of upper- and lower-horizontal currents. In a certain bias range, a type A breather is formed. Then, $\tilde{I}_L$ is decreased and I_B is increased, while the voltage drop V_{3-4} is kept constant. While sweeping current-voltage characteristics, the voltage V_{5-6} between the edge nodes 5 and 6, as well as the upper- and lower-horizontal voltages, V_{4-6} and V_{3-5} were monitored.

Figure 2 shows a measured current-voltage characteristics of the Josephson ladder in the presence of a $B1$ breather at the central site. This state was created in the standard way, which was reported earlier [7,10]. The normalized bias current $\gamma = I/I_{c,\mathrm{tot}}$ is the ratio of the overall ladder bias I and the ladder critical current $I_{c,\mathrm{tot}} = 11 I_c = 225\,\mu$A. The normalized voltage is $v_v = V_{3-4}/V_0$, where $V_0 = \Phi_0/(2\pi)\omega_p = 84.3\,\mu$V.

The curve exhibits a linear branch in the upper right region ($v_v > 13$) which continues at $v_v \approx 10$ and at $v_v \approx 5$. The linear branch is merged with dominant, almost vertical steps around $v_v \approx 11.4$ (M region), and around $v_v \approx 5.7$ (L region). An additional step occurs at $v_v \approx 3$ (K region). This lowest branch corresponds to a type $A1$ breather that has been proven by measuring upper- and lower-horizontal voltages. All steps show hysteretic behavior when sweeping the bias current up and down. Voltage jumps occur when the bias is increased to the top of the step and when the bias is decreased at its bottom, as indicated by arrows. After decreasing the bias current in the K branch, the voltage jumps to zero, hence, all junctions migrate into the S state. A fine structure is present on the voltage steps L and M, as shown in the insets.

The voltage jumps shown in Fig. 2 are not always reproducible. Occasionally, a state with larger size is picked up by lowering the bias on the M branch (a part of such a branch is shown in the figure around $\gamma \approx 0.35$ and $v_v \approx 10$). The jumps from the ''top'' parts of the steps sometimes also result in larger breather states, or even in the homogeneous whirling state of the whole ladder. From the top of the L step, the voltage may jump to the M step, or to the linear branch at larger voltage (not shown in the figure).

The K region, as shown in Fig. 2, is obtained very rarely by lowering the bias current from the L branch. Typically, the S state of the ladder is picked up instead. Using the alternative breather-creation method mentioned above, a type $A1$ breather can be created in a more controlled way. Therefore, the K region may be studied in detail.

To complete this section of experimental results, we discuss the measured voltage positions of the observed steps. Most notably, the voltage positions of observed steps are at nearly integer multiples of each other. We observe the K step at $v_K = 2.90$, the L step at $v_L \approx 5.77 = 1.99 v_K$, and the M step at $v_M \approx 11.45 = 1.98 v_L = 3.95 v_M$.

The measured step voltages also map remarkably well to the analytic linear mode dispersion relation: From Eq. (4) we calculate the frequency $\omega_+(l=2) = 2.84$ for the lowest mode with a node in the center of the ladder, where the breather is excited. This frequency agrees well with the measured normalized voltage of the K step [$v_K = 1.02 \omega_+(l=2)$], as well as the L and M steps, which coincide with the double and the fourfold ω_+.

We argue that the observed voltage steps are resonances of the breather with cavity modes of the ladder. They occur when the frequency of a whirling junction (either vertical, or horizontal) coincides with one of the eigenfrequencies of the junction array, or its integer multiples.

V. NUMERICAL INVESTIGATIONS

To obtain more detailed information about the nature of the experimentally observed voltage steps, we numerically integrated the set of equations (2) by a standard fifth-order Runge-Kutta method with adaptive step-size control by Cash-Karp parameters [19]. Breather solutions were generated by starting the simulation from proper initial conditions that lead to the relaxation of the system into the desired state.

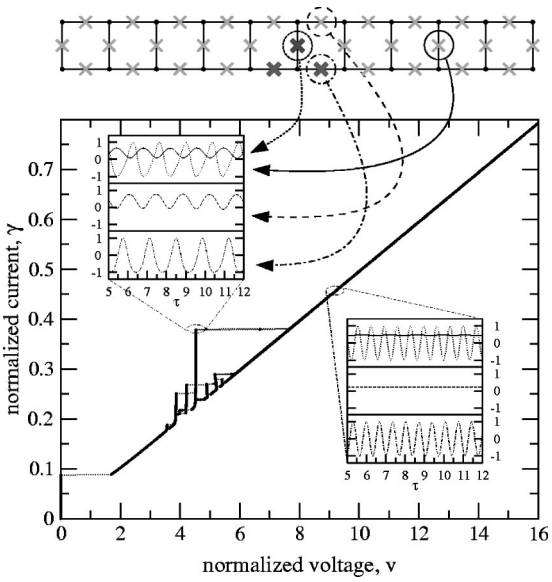

FIG. 3. Simulated current-voltage characteristics of an $A1$ breather showing resonances in the K region. The insets show the temporal evolution of the normalized supercurrent $\sin\varphi_9$ (solid line), $\sin\varphi_6$ (dotted line), $\sin\tilde{\psi}_6$ (dashed line), and $\sin\psi_6$ (dash-dotted line).

The breathers were placed into the center of the ladder, e.g., between cells 5 and 6 for a ten-cell ladder.

The numerically found current-voltage characteristics show the bias current per ladder node γ, versus the normalized vertical junction voltage $v = v_v = \langle \dot{\varphi}_n \rangle$. Details about the numerical routines we used may be found in Ref. [15].

We simulated a ten-cell anisotropic Josephson ladder with open boundaries and $\alpha = 0.025$ and $\eta = 0.49$. We have chosen to present here simulations performed at $\beta_L = 0.37$ that show a rich structure of cavity resonances and supplement the experimental picture. Current-voltage curves were obtained for both type $A1$ and $B1$ breathers. The initial conditions were chosen for a bias current of $\gamma = 0.8$. After the relaxation of the system, the current was decreased down to zero by decrements of $\Delta\gamma < 10^{-4}$. When voltage jumps were found, the bias was increased to trace out resonances, exactly in the way as experimental curves were taken.

Figure 3 presents numerically obtained current-voltage characteristics for an $A1$ type breather. There is ohmic behavior for $v \gtrsim 6$, but several steps occur for $3.5 < v < 6$. The ohmic branch continues for lower voltages, and the ladder jumps to the S state at $\gamma = 0.089$ and $v = 1.69$. The steps were traced out by increasing γ from the bottom of the steps. Increasing the bias on the top of a step leads to a voltage jump, either towards the ohmic branch, or (for the lower steps) to a higher step. Note that the type A solution is preserved after voltage jumps; a transition to a type B state is not yet observed in this simulation.

The insets in Fig. 3 show the time evolution of selected supercurrents (equal to the sine of the phase difference) in the ladder for a bias point on the ohmic branch and for a point at the peak of the most dominant step. On the ohmic branch at $v = 9.19$, the picture is easily understood: At the breather site, the vertical junction phase φ_6 is increasing lin-

TABLE I. Numerical and analytical voltage positions of steps observed in Fig. 3.

Step No.	Voltage	(q_l)	$\omega_+(q_l)$
1	3.57	2	3.59
2	3.87	4	3.90
3	4.22	6	4.26
4	4.53	8	4.58
5	4.88	unidentified	
6	5.17	unidentified	
7	5.42	unidentified	

early in time, so are the horizontal phases ψ_6 and ψ_5 (the latter is not shown in the picture). Consequently, the super-current swings from -1 to 1. The other vertical junctions in the ladder are in the static state, with $\varphi_n = \arcsin \gamma$.

The situation is changed dramatically on the voltage step, which can be clearly seen from the upper-left inset. The horizontal and vertical junctions *outside* the breather oscillate at a frequency that is identical to the breather frequency Ω. A view at the spatial phase profile in the ladder reveals that a standing wave has formed. The different voltages of steps may be understood as resonances of the breather with cavity modes of different wave-numbers q_l.

In Table I, we list the voltage positions of the observed steps from Fig. 3, as well as the frequencies (which correspond to the normalized voltage) calculated from Eq. (4) using $\gamma = 0.3$. We note that only the lower four, clearly pronounced steps from the simulation may be mapped to the dispersion relation. There, only the even cavity modes are excited. This might be due to the requirement of a wave node at the breather position, which is the center of the ladder. Placing the breather away from the system center allows for the excitation of even and odd cavity modes also, which we checked in additional simulations. The upper-three steps that show a peculiar back-bending shape do not coincide with any of the cavity mode frequencies. In fact, their voltage ranges even above the ω_+ band, which lies between $3.47 < \omega_+ < 4.78$. Further inquiry on the nature of these resonances is required.

As may be expected, the picture gets more complex for the type $B1$ breather. The frequencies of the vertical and horizontal whirling junctions differ, thus, more resonances with cavity modes may be observed. In Fig. 4, we plot the simulated current-voltage characteristics for a type $B1$ breather in a Josephson ladder with parameters as described above. On this curve, three regions with resonant voltage steps are present, which we identify as *K*, *L*, and *M*. As for the type $A1$ breather, voltage jumps from the top of steps may target on the ohmic branch, or on neighboring resonance steps, depending on their current amplitude. We frequently observe an increase of the breather size after voltage jumps, mainly from the resonances in the *L* and *M* regions. This behavior was also observed in the experiments.

Information on the spatiotemporal dynamics on some voltage steps may again be obtained from the insets of Fig. 4. The supercurrents are plotted as in the insets from Fig. 3. It is clear that for the *K* resonances, the *vertical* junction frequency Ω_v is equal to the lattice frequency ω_+, which is represented by the oscillations of φ_9, while the horizontal junction frequency Ω_h is half of this value. In contrast, for the *L* resonances $\Omega_v = 2\omega_+$, while the horizontal frequency $\Omega_h = \omega_+$. As for the type A breather, the different steps in the *K* and in the *L* range correspond to the locking of the respective breather frequencies to different cavity modes given by Eq. (5). Similar to the A breather case, we observe additional resonances in the *L* range around $10 < v < 10.5$, which show a very strong back bending. The steps in the *K* region and lower steps from the *L* region lie well within the ω_+ band and $2\omega_+$ band, respectively. The three upper steps in the *L* region are above the $2\omega_+$ band and cannot be identified as simple cavity resonances.

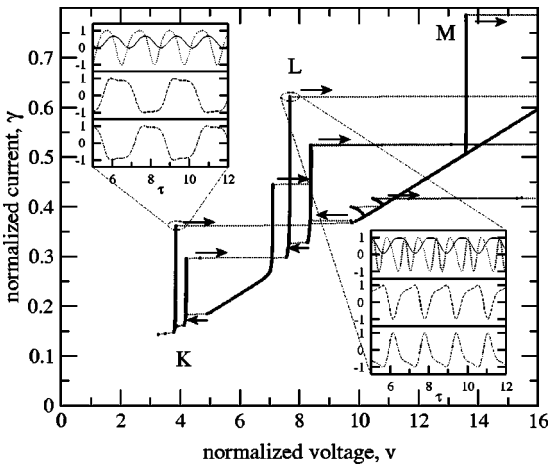

FIG. 4. Simulated current-voltage characteristics of a $B1$ breather with resonances (*K*, *L*, and *M* regions). The insets show the same super-current time evolutions as in Fig. 3.

An additional resonant voltage step named *M* is observed at $v = 13.5$. Here, voltage is close to $\Omega_h \approx 2\omega_+$ and $\Omega_v \approx 4\omega_+$. Therefore, it might be identified as a parametric resonance of the breather and the linear waves, as described in Ref. [12]. However, the *M* step lies within the $3\omega_+$ band, but slightly below the $4\omega_+$ band. The observed steps *K* and *L* may be mapped to the dispersion relation similar to the type $A1$ breather resonances. The results are shown in Table II. The peculiar *M* step, which is observed both in simulation

TABLE II. Numerical and analytical voltage positions of steps observed in Fig. 4.

Step	Voltage	Multiplier	Base voltage	(q_l)	$\omega_+(q_l)$
$K1$	3.86	1	3.86	4	3.90
$K2$	4.21	1	4.21	6	4.26
$L1$	7.11	2	3.55	2	3.59
$L2$	7.68	2	3.84	4	3.90
$L3$	8.39	2	4.19	6	4.26
$L4$	9.72	2	4.86	unidentified	
$L5$	9.73	2	4.87	unidentified	
$L6$	10.46	2	5.23	unidentified	
M	13.58	4	3.40	unidentified	

and experiment, cannot be explained within our easy model. It has to be noted that the *M* step is obtained in our simulation only in the absence of any numerical noise, or small deviations from the initially symmetric $B1$ breather state. Preliminary investigations indicate that the resonance *M* is accompanied by an unstable symmetric $B1$ state [20].

The discussed resonances in the *K*, *L*, and *M* range are very similar to that observed in experiment. Due to the different values of β_L, the normalized voltage positions are different in experiment and simulation. The respective step positions are however predicted rather precisely from the analytic dispersion relation (4). Additional simulations were performed using $\beta_L = 0.62$, which closely conforms to the experimental value. These show resonant steps only at the low end of the ω_+ band, as observed in the experiment.

VI. CONCLUSIONS

We presented experimental observation of resonances between discrete breathers and extended linear electromagnetic excitations of Josephson ladders. Their resonant interaction leads to large voltage steps on current-voltage characteristics of the ladders.

Numerical simulations that we also performed show a good agreement with experiment. The dispersion relation for small-amplitude linear waves allows to rather precisely predict both measured and simulated resonance positions.

Simulations show multiple discrete steps at nearby voltage positions. This circumstance is explained by the locking of the breather frequency to the discrete linear wave spectrum of the ladder. Type B breathers comprehend at least two internal main frequency components. As expected, the current-voltage characteristics of such states shows sets of steps in separated voltage ranges.

Experiments, which were performed at a higher value of the discreteness, showed resonances between breathers and linear modes only for small wave vectors. This behavior is reproduced by simulations conducted at the corresponding larger discreteness parameter. In experiment, a fine structure was observed *superimposed* on the resonance branches. This feature is not yet understood and also not reproduced in simulations.

Future experiments should survey the existence ranges of breather resonances. Different lattice oscillation wave vectors could be stabilized by tuning the external magnetic field, hence, breather resonances may be expected to shift in voltage with the field. Furthermore, the direct observation of the wave numbers should be possible by low-temperature scanning laser microscopy [7]. Such experiments have been already done for Fiske steps in distributed superconducting structures [21,22]. A spectroscopy of the resonant breather states might lead to insight on phonon-breather interaction in Josephson ladders. In addition, the radiation absorption and emission from resonant breathers in ladders might not only be used as a diagnostic tool, but possibly also lead to interesting applications such as submillimeter wave antennas or sources.

ACKNOWLEDGMENTS

We are indebted to M.V. Fistul, S. Flach, A. Kemp, J.J. Mazo, A.E. Miroshnichenko, F. Pignatelli, and Y. Zolotaryuk for fruitful discussions. We especially thank J.J. Mazo and A.E. Miroshnichenko for sending us their latest work prior to publication. This work was supported by the Deutsche Forschungsgemeinschaft (DFG) and by the European Union under the RTN Project No. LOCNET HPRN-CT-1999-00163.

[1] S. Aubry, Physica D **103**, 201 (1997).
[2] S. Flach and C. R. Willis, Phys. Rep. **295**, 181 (1998).
[3] H. S. Eisenberg, Y. Silberberg, R. Morandotti, A. R. Boyd, and J. S. Aitchison, Phys. Rev. Lett. **81**, 3383 (1998).
[4] B. I. Swanson, J. A. Brozik, S. P. Love, G. F. Strouse, A. P. Shreve, A. R. Bishop, W.-Z. Wang, and M. I. Salkola, Phys. Rev. Lett. **82**, 3288 (1999).
[5] U. T. Schwarz, L. Q. English, and A. J. Sievers, Phys. Rev. Lett. **83**, 223 (1999).
[6] E. Trías, J. J. Mazo, and T. P. Orlando, Phys. Rev. Lett. **84**, 741 (2000).
[7] P. Binder, D. Abraimov, A. V. Ustinov, S. Flach, and Y. Zolotaryuk, Phys. Rev. Lett. **84**, 745 (2000).
[8] K. Likharev, *Dynamics of Josephson Junctions and Circuits* (Gordon and Breach Science, New York, 1986).
[9] L. M. Floría, J. L. Marín, P. J. Martínez, F. Falo, and S. Aubry, Europhys. Lett. **36**, 539 (1996).
[10] P. Binder, D. Abraimov, and A. V. Ustinov, Phys. Rev. E **62**, 2858 (2000).
[11] E. Trías, J. J. Mazo, A. Brinkman, and T. P. Orlando, Physica D **156**, 98 (2001).
[12] A. E. Miroshnichenko, S. Flach, M. V. Fistul, Y. Zolotaryuk, and J. Page, Phys. Rev. E **64**, 066601 (2001).
[13] R. T. Giles and F. V. Kusmartsev, Phys. Lett. A **287**, 289 (2001).
[14] P. Caputo, M. V. Fistul, A. V. Ustinov, B. A. Malomed, and S. Flach, Phys. Rev. B **59**, 14050 (1999).
[15] M. Schuster, Diploma thesis, University of Erlangen, 2000.
[16] G. Grimaldi, G. Filatrella, S. Pace, and U. Gambardella, Phys. Lett. A **223**, 463 (1996).
[17] Hypres Inc., Elmsford, NY.
[18] This nice idea was proposed to us by A. Kemp.
[19] W.H. Press, *Numerical Recipes in C: The Art of Scientific Computing*, 2nd ed. (Cambridge University Press, Cambridge, England, 1999), Chap. 16.
[20] A. E. Miroshnichenko (private communication).
[21] B. Mayer, T. Doderer, R. P. Huebener, and A. V. Ustinov, Phys. Rev. B **44**, 12463 (1991).
[22] D. Quenter *et al.*, Phys. Rev. B **51**, 6542 (1995).